JOURNAL OF GEOPHYSICAL RESEARCH, VOL. 96, SUPPLEMENT, PAGES 3151–3163, FEBRUARY 28, 1991

An Equilibrium Model for the Coupled Ocean-Atmosphere Boundary Layer in the Tropics

C.-H. SUI AND K.-M. LAU

Laboratory for Atmospheres, NASA Goddard Space Flight Center, Greenbelt, Maryland

ALAN K. BETTS

Middlebury, Vermont

A coupled model is used to study the equilibrium state of the ocean-atmosphere boundary layer in the tropics. The atmospheric model is a one-dimensional thermodynamic model for a partially mixed, partly cloudy convective boundary layer (CBL), including the effects of cloud-top subsidence, surface momentum and heat (latent and sensible) fluxes, and realistic radiative transfer for both shortwaves and longwaves (Betts and Ridgway, 1988; 1989). The oceanic model is a thermodynamic model for a well-mixed layer, with a closure constraint based on a one-dimensional turbulent kinetic energy (TKE) equation following Kraus and Turner (1967). Results of several sets of experiments are reported in this paper. In the first two sets of experiments, with sea surface temperature (SST) specified, we solve the equilibrium state of the coupled system as a function of SST for a given surface wind (case 1) and as a function of surface wind for a given SST (case 2). In both cases the depth of the CBL and the ocean mixed layer (OML) increases and the upwelling below the OML decreases, corresponding to either increasing SST or increasing surface wind. The deepening of the equilibrium CBL is primarily linked to the increase of CBL moisture with increasing SST and surface wind. The increase of OML depth and decrease of upwelling are due to a decrease of net downward heat flux with increasing SST and the generation of TKE by increasing wind. In another two sets of experiments, we solve for the coupled ocean-atmosphere model iteratively as a function of surface wind for a fixed upwelling (case 3) and a fixed OML depth (case 4). SST falls with increasing wind in both cases, but the fall is steeper in case 4, because the OML depth is fixed, whereas in case 3 the depth is allowed to deepen and the cooling is spread over a larger mass of water. The decrease of evaporation with increasing wind in case 4 leads to a very dry and shallow CBL. Results of further experiments with surface wind and SST (upwelling) prescribed as a function of longitude similar to the observed values across the Pacific show that the model gives realistic gradients of mixed-layer depth and upwelling (SST). This work suggests that the equilibrium state of the coupled system is very sensitive to the coupling of the boundary layers. Special efforts are needed to incorporate physical processes in the CBL and OML in coupled models.

1. INTRODUCTION

Recent studies of El Niño/Southern Oscillation (ENSO)-related phenomena have generated great interest in the coupled dynamics of the tropical ocean and global atmosphere (TOGA). Theoretical and modeling studies have shed light on some fundamental mechanisms responsible for the interannual variations in idealized coupled systems. Simulations of the long-term behavior of the coupled ocean-atmosphere, based on coupled general circulation models (GCMs), however, have often been hampered by a serious "climate drift" problem [e.g., *Latif et al.*, 1988, and references therein]. This indicates that the mean or equilibrium state of the coupled system needs to be studied first, before the perturbed climate state can be understood. Since the source of the "climate drift" problem is directly related to the interactive quantities like surface wind, air and sea temperature, and heat fluxes, it is necessary to seek a better understanding of the processes maintaining the boundary structure near the interface of the tropical ocean and atmosphere.

The most well defined boundary layer in the tropical atmosphere is observed over the eastern and central Pacific, where subsidence and low-level easterly trade winds are dominant. The atmospheric boundary layer in this region is maintained by heating or cooling effects due to subsidence, radiation, and surface fluxes [e.g., *Betts and Ridgway*, 1989]. On the other hand, the depth of the well-mixed oceanic boundary layer in this region is known to have marked zonal variations, which are positively correlated with the sea surface temperature (SST) [e.g., *Meyers*, 1979]. The oceanic mixed layer is maintained by surface momentum and heat fluxes, and upwelling and entrainment through the thermocline.

In this paper, we adopt the atmospheric convective boundary layer (CBL) model developed by *Betts and Ridgway* [1988, 1989], and couple it to an ocean mixed layer (OML) model to study the equilibrium state of the coupled system in the tropics, particularly in the Pacific region. A similar approach was adopted by *Sarachik* [1978]. A schematic illustration of the characteristics of the coupled system in an east-west cross section near the equator is shown in Figure 1.

In the relatively smaller region of the ascending branch of the atmospheric circulation in the tropical western Pacific, the coupled ocean-atmosphere system is characterized by weak surface wind, warm sea surface temperature, a deep oceanic mixed layer, and deep atmospheric convection. The coupled processes in this region are more complicated. The

Paper number 90JC01776.
0148-0227/91/90JC-01776$05.00

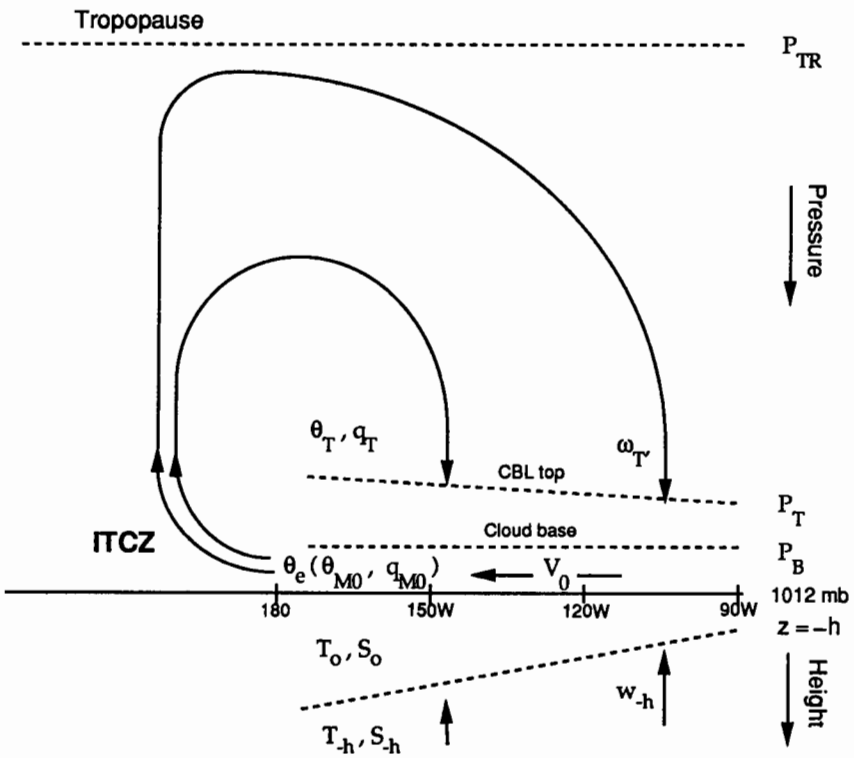

Fig. 1. A schematic illustration of characteristics of the coupled CBL and OML in the tropical Pacific along the equator.

upcoming TOGA/Coupled Ocean-Atmosphere Response Experiment (COARE) is aimed at providing a better understanding of the coupled processes in this region. Because the subsiding branch of the tropical atmospheric general circulations and the ascending motion of the Intertropical Convergence Zone (ITCZ) are linked through moisture in the boundary layer, the work reported in this paper is an essential part of the TOGA-related study and is a complement to TOGA-COARE. As evident in the TOGA-COARE Science Plan [*U.S. TOGA-COARE Science Working Group*, 1989], the scientific issues facing COARE are extremely complex. No single approach is adequate to tackle the problems involved. The present approach is intended only as a first step toward a more realistic model to study the relative importance of radiation, cloud, wind, evaporation, and precipitation on the maintenance of the coupled system in the tropical Pacific region.

In the following, the atmospheric and oceanic boundary layer models are introduced in sections 2 and 3, respectively. In sections 4 and 5, we present results of sensitivity experiments showing the relative importance of SST, surface wind, radiation, atmospheric subsidence, and oceanic upwelling in maintaining the boundary layers in the coupled system. Summary, discussion, and conclusion are given in sections 6, 7, and 8, respectively.

2. Atmospheric Convective Boundary Layer Model

2.1. *Basic Equations*

The atmospheric CBL model was developed by *Betts and Ridgway* [1988, 1989] (hereafter referred to as BR1, BR2), based on the mixing line representation of the bulk thermodynamic properties of the partially cloudy CBL. The CBL structure in the broad subsiding region of tropical Pacific is characterized by a fairly uniform cloud base near 950 mbar and an inversion above the top of the cloud layer near 800 mbar [*Betts and Albrecht*, 1987]. Such an equilibrium CBL is maintained primarily by radiative cooling, subsidence, convective transports, and surface latent and sensible heat fluxes (see Figure 2 for a schematic illustration). A quantitative description of this balance can be expressed by the steady, horizontally homogeneous, heat and moisture budget equations vertically integrated through the CBL, from surface (at pressure p_0) to inversion top (at pressure p_T),

$$\underset{\text{subsidence warming}}{\omega_{T'}(\theta_T - \theta_{M0})} - \underset{\text{radiative cooling}}{(g\theta/c_pT)\Delta N_T} + \underset{\text{surface heat flux}}{(g/c_p)H_s} = 0 \tag{1}$$

$$\underset{\text{subsidence drying}}{\omega_{T'}(q_T - q_{M0})} + \underset{\text{surface moisture flux}}{(g/L)H_e} = 0 \tag{2}$$

where $\omega_{T'}$ is a parameter proportional to subsidence, θ_T and q_T are the potential temperature (θ) and mixing ratio (q) at CBL top, respectively; θ_{M0} and q_{M0} are defined at 2 mbar above the surface; $\Delta N_T(=N_T - N_0)$ is the difference of net radiative flux at the CBL top (N_T) and surface (N_0); H_s, H_e are the surface sensible and latent heat fluxes; g, c_p, and L are the constant of the gravity, specific heat, and latent heat, respectively; and $(g\theta/c_pT)$ is assumed a constant. To derive (1) and (2), the internal variations of divergence within the CBL are ignored (see BR2 for more details).

The surface fluxes are parameterized by the bulk formulas as

$$H_s/c_p = \omega_0(\theta_o - \theta_{M0})/g \tag{3}$$

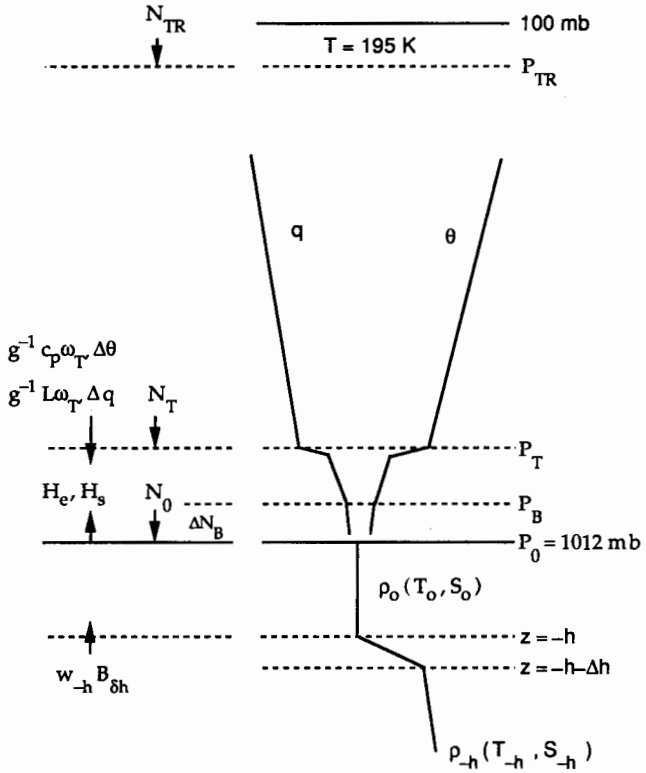

Fig. 2. A schematic structure of the coupled CBL-OML model and important thermodynamic fluxes maintaining the coupled boundary layer.

$$H_e/L = \omega_0(q_o - q_{M0})/g \tag{4}$$

where θ_o and q_o are given at the sea surface temperature and pressure (1012 mbar), assuming saturation, and ω_0 is a surface wind parameter, defined as

$$\omega_0 = \rho_a g c_H V_0 \tag{5}$$

where ρ_a and V_0 are surface air density and wind speed, respectively, and c_H is a surface transfer coefficient.

Among the variables in the system of equations (1)–(4), ω_0 is specified because it cannot be diagnosed in the present model, and q_T can be either specified or linked to low-level equivalent potential temperature (θ_e), found from θ_{M0} and q_{M0} (q_T is specified in this study). All the radiative fluxes are computed via a radiation model and are regarded as known variables. For a given T_o (therefore θ_o and q_o), there are still six unknowns in the above CBL equations: $\omega_{T'}$, θ_T, θ_{M0}, q_{M0}, H_s, and H_e. If $\omega_{T'}$ is specified, an extra energy balance constraint is needed to close the system. BR2 choose to couple the surface heat flux to the radiative cooling for the subcloud layer by assuming

$$H_s = -\Delta N_B/(1 + \kappa) \tag{6}$$

where $\kappa = 0.25$ and $\Delta N_B(=N_B - N_0)$ is the difference between net radiative flux at the surface and cloud base (N_B). BR2 discuss the limitations of their model for climate studies further.

The radiative fluxes are crucial physical quantities in the CBL model. A radiative transfer model, developed by *Harshvardhan et al.* [1987], is adopted to calculate the one-dimensional radiative fluxes for a partly cloudy CBL (CBL cloud fraction is specified at 0.25 for all experiments in this paper), based on the thermodynamic profiles below and above the CBL top up to 100 mbar. Some related quantities specified in this study are listed in Table 1.

TABLE 1. Basic Model Parameters

Parameter	Value
Solar zenith angle	51.74°
Surface albedo	0.07
Incoming SW flux	1360.3 W m^{-2}
Atmosphere CBL parameters	
Cloud fraction	25%
Cloudy thermodynamic profiles	β_c = 0 (subcloud); 0.6 (cloud layer)
Clear air thermodynamic profiles	β_u = 0.2 (subcloud); 1.2 (cloud layer)
Surface pressure	p_a = 1012 mbar
Mixing ratio just above CBL	q_T = 4.8 g kg^{-1}
Subsidence parameter	$\omega_{T'}$ = 0.05 Pa s^{-1}
Ocean mixed layer parameters	
$T_o - T_{-h}$	1.5°
Extinction coefficient	ε = 0.2 m^{-1}
Fraction of generation rate of TKE due to work done by wind mixing	m = 0.0012
Coefficient of thermal expansion	$\alpha = 297 \times 10^{-6}$
Coefficient of saline contraction	$\lambda = 0.7 \times 10^{-3}$

2.2. *Solution Procedures*

For a specified sea surface temperature (therefore θ_o and q_o) and wind parameter (ω_0), a set of equilibrium solutions can be obtained by repeating the following procedures 1–4 until a convergent solution is obtained:

1. Starting from given standard tropical temperature and humidity profiles, an initial field of radiative fluxes (ΔN_B, ΔN_T) is first calculated. Unknowns H_s, H_e, θ_{M0}, θ_T, and q_{M0} can then be computed from (1), (2), (3), (4) and (6).
2. Cloud base pressure (p_B) is defined as the lifting condensation level, determined from θ_{M0} and q_{M0}, and cloud top pressure p_T is found by solving $\theta_{es}(\theta_T, p_T) = \theta_e$ (fixed at 347°K), where θ_{es} is the saturation equivalent potential temperature above the CBL.
3. Between (θ_{M0}, q_{M0}) near the ocean surface and (θ_T, q_T) just above the CBL, a mixing line can be computed and the thermodynamic properties of all the air in the CBL are assumed to lie on this mixing line. The thermodynamic profiles for clear and cloudy air within the CBL are constructed by specifying different profiles for a parameter β, where β is the change of saturation level with pressure along the mixing line [*Betts*, 1982, 1985]. For the clear air, BR2 specify the value of β (denoted as βu) = 0.2, 1.2 below cloud base and above cloud base, respectively. For the cloudy CBL profiles, BR2 specify the value of β (denoted as β_c) = 0.0, 0.6 below cloud base and in the cloud layer, respectively. These values were based on earlier observational studies [*Betts and Albrecht*, 1987].
4. The tropospheric temperature is assumed to follow a specified moist θ_{es} adiabat from CBL top to the tropopause (defined as the point where this θ_{es} adiabat reaches 195°K), the moisture profile above the CBL is found by interpolation between values at the CBL top (q_T) and the tropopause. Temperature between 100 mbar and the tropopause is assumed to be 195°K.

5. A new field of radiative fluxes is computed based on the vertical profiles of thermodynamic properties obtained from procedures 1 through 4.

3. Oceanic Mixed Layer Model

Following *Kraus and Turner* [1967], the idealized oceanic mixed layer is modeled as a vertically homogeneous layer (of depth h) on top of a deep ocean with a stably stratified density discontinuity at the interface (see the schematic diagram Figure 2). Horizontal advection and mixing are assumed to be much less effective and are ignored in this work. Convergence, integrated through the mixed layer, is included by specifying a vertical velocity (w_{-h}) at some depth just below the bottom of the mixed layer. The input of thermal and mechanical energy through the top and bottom boundaries is assumed to be redistributed uniformly within the layer by turbulent mixing. The mixed-layer temperature (T_o) and salinity (S_o) are governed by the vertically integrated thermodynamic and salinity equations:

$$h\frac{dT_o}{dt}+\Lambda\left(w_{-h}+\frac{dh}{dt}\right)(T_o-T_{-h})= -\frac{1}{\rho_o c}(R_0^*-R_{-h}^*+I_0+H_s+H_e) \quad (7)$$

$$h\frac{dS_o}{dt}+\Lambda\left(w_{-h}+\frac{dh}{dt}\right)(S_o-S_{-h})=\frac{1}{\rho_o}(E-P)S_o \quad (8)$$

(ρ_o and c are the density and specific heat of the ocean mixed layer). Heat fluxes at the top of the mixed layer include net downward flux of solar radiation (R_0^*; here the asterisk superscript denotes a quantity which is negative downward) and net upward longwave radiation (I_0), and turbulent flux of sensible heat (H_s) and latent heat (H_e). R_{-h}^* is the net solar radiative flux at the depth $z=-h$, as defined in (11) below. Evaporation (E) and precipitation (P) are the source (or sink) terms for salinity. Note that

$$H_e=LE,\ N_0=-(R_0^*+I_0) \quad (9)$$

Through the bottom of the mixed layer, upwelling and turbulent mixing can occur as colder, saltier water from below (characterized by T_{-h}, S_{-h}) is advected and entrained upward when ($w_{-h}+dh/dt$) is positive. When ($w_{-h}+dh/dt$) is negative, entrainment must cease. Therefore, Λ is introduced in the above equations such that it will be set to 1 if ($w_{-h}+dh/dt$) is positive and 0 otherwise. See the appendix and the following discussions for more details.

A third equation is needed to close the system (7)–(8). Following *Kraus and Turner* [1967], the vertically integrated turbulent kinetic energy equation, as derived in the appendix, gives

$$\Lambda\left(w_{-h}+\frac{dh}{dt}\right)=\frac{2}{hB_{\delta h}}\left[mu_*^3+\frac{h}{2}F_{B0}+\frac{g\alpha}{\rho_o c}\left(\frac{h}{2}R_0^*+\frac{h}{2}R_{-h}^*-\int_{-h}^{0}R^*\,dz\right)\right] \quad (10)$$

where α is the coefficient of thermal expansion; m is the fraction of generation rate of TKE due to work done by wind mixing; F_{B0} is the buoyancy flux given in (A5); and $B_{\delta h}$, given in (A12), is the buoyancy due to discontinuous changes of temperature and salinity across the base of the mixed layer. The radiative flux in the ocean mixed layer can be computed by

$$R^*(z)=R_0^*e^{\varepsilon z} \quad (11)$$

where ε is the extinction coefficient. In (10), the first and second terms on the right-hand side represent the generation of turbulent kinetic energy (TKE) by wind, and the buoyancy forcing due to surface momentum and heat fluxes, respectively. The remaining terms denote the reduction of TKE due to solar radiative heating. Entrainment occurs only when there is net generation of TKE by the forcing terms mentioned above and ($w_{-h}+dh/dt$) is positive. When the production of turbulent energy within the mixed layer is insufficient to maintain entrainment at the bottom of the mixed layer, entrainment processes can not occur and ($w_{-h}+dh/dt$) = 0 or is negative.

Such an OML model had been used by *Denman* [1973] and *Kim* [1976] to study the time-dependent solution of the ocean. *Miller* [1976] tested the salinity effect in the mixed-layer model. Recently, *Chu and Garwood* [1989] used a similar model to study cloud-OML feedback.

Since we focus on the equilibrium solution in the subsiding branch in this work, only the steady form of (7) and (10) are used in the present model. The effect of salinity is neglected, because precipitation is not considered. The inclusion of precipitation in the atmospheric model and salinity in the OML is an ongoing modification of the coupled model in our next approach to study the coupled dynamics in the tropical Pacific region. In the two OML equations, all the surface fluxes are coupled to the atmospheric CBL and the difference of T_o-T_{-h} is assumed constant. Therefore only three primary variables, T_o, h, and w_{-h}, are considered. One of them has to be given in the coupled solution. Some basic parameters are listed in Table 1.

4. Solutions for Prescribed SST in the Coupled Model

In this section, we shall investigate the response of the CBL-OML model to specified SST and surface wind. Since both SST and surface wind are given, the CBL and OML are effectively decoupled. Here the atmospheric boundary layer structure and surface fluxes at the top of the mixed layer (R_0^*, I_0, H_s, H_e) can be obtained by the CBL model. The oceanic upwelling is determined by the thermodynamic balance (7), and the mixed layer depth is obtained from the TKE (turbulent kinetic energy) constraint (10).

4.1. *Equilibrium States as a Function of SST*

For a given surface wind parameter, $\omega_0=0.1$ Pa s^{-1} (corresponding to a surface wind of 6.7 m s^{-1}), and a set of SSTs representative of that of the Pacific, the CBL top and base and the corresponding oceanic mixed-layer depth are shown in Figures 3*a* and 3*b* as a function of SST. The change of upwelling (w_{-h}) required to maintain the OML is shown in Figure 3*c*. With increasing SST, the cloud base remains almost constant at 950 mbar, while cloud top rises rapidly. The mixed layer depth increases from 30 to 100 m, and upwelling decreases from 0.90×10^{-5} to 0.27×10^{-5} m s^{-1} as SST increases from 24° to 27°C. The magnitude of these

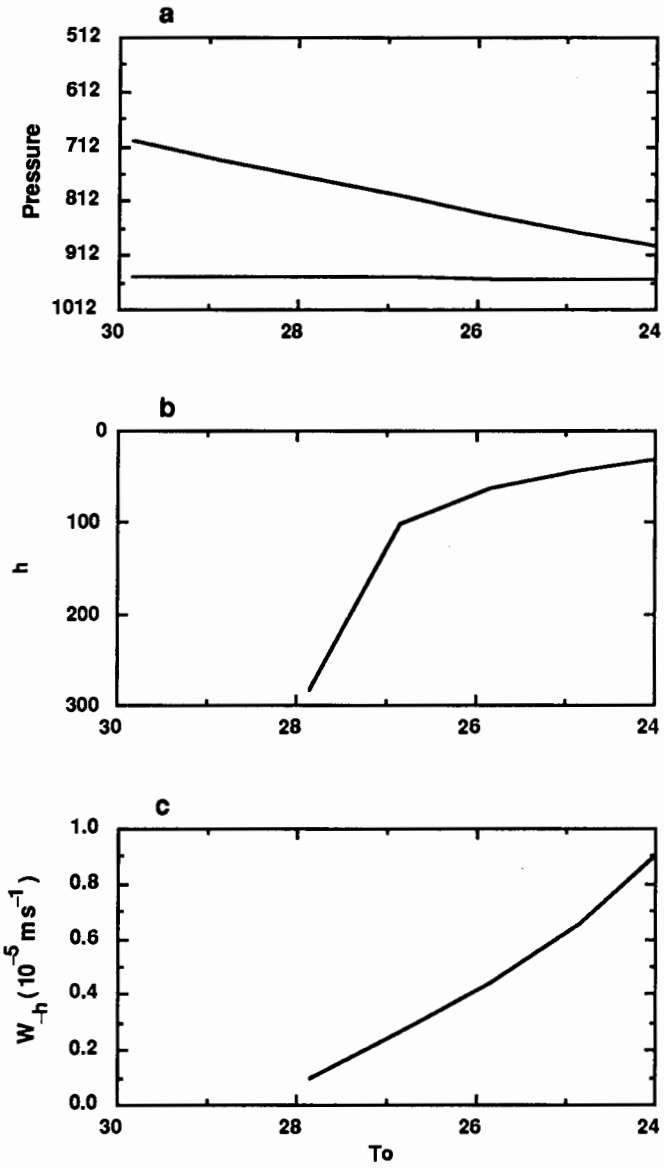

Fig. 3. Equilibrium solution as a function of SST for (*a*) cloud base and CBL top, (*b*) mixed-layer depth, and (*c*) upwelling below the OML, for prescribed SST at $\omega_0 = 0.1$.

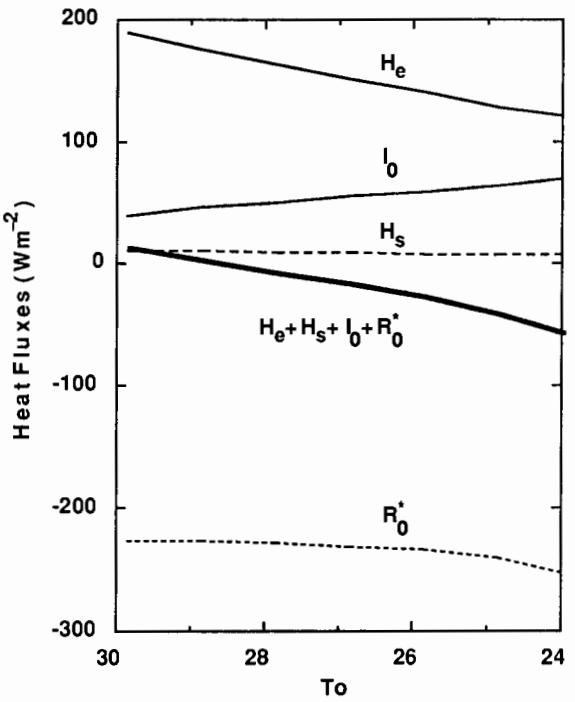

Fig. 4. Surface fluxes of latent heat (H_e), sensible heat (H_s), net upward longwave radiation (I_0), net downward solar radiation (R_0^*), and total heat flux for equilibrium solution as a function of SST, for prescribed SST at $\omega_0 = 0.1$.

solutions is in general agreement with observations, as discussed later. But for SSTs warmer than 27°C, mixed-layer depth becomes unrealistically large. This is because the surface wind speed over the warm Pacific is generally weaker than the value (6.7 m s^{-1}) used in this experiment.

The variations of surface energy fluxes are shown in Figure 4. It shows that surface energy budget consists of a very delicate balance among the various flux terms. The most significant changes with SST are found in latent heat (H_e), solar (R_0^*), and longwave (I_0) radiative fluxes. Both solar and longwave radiative fluxes decrease (in magnitude), while latent heat flux increases with increasing SST. The change of latent heat is due to the increase of Δq with rising SST (see section 6). Solar radiative fluxes decrease with increasing SST, because of increased reflection caused by more cloud droplets in the CBL. The net longwave radiative flux decreases with increasing SST because of the stronger downward emittance from increased water vapor in the subcloud layer is greater than the increase in upward radiation from the sea surface.

In the OML model, the mixed-layer depth is obtained from the TKE (turbulent kinetic energy) constraint (10) if T_o is known. Generation of TKE due to mechanical stirring by the surface stress tends to deepen the mixed layer. Upward surface heat flux due to H_s, H_e, and I_0, by cooling ocean surface, creates downward buoyancy and tends to deepen the mixed layer. The downward solar radiative flux, on the other hand, reduces the buoyancy and increases the mean potential energy of the system by warming the ocean surface. It opposes the deepening of the mixed layer.

At a fixed surface wind, the change of mixed layer depth as function of SST is all determined by buoyancy forcing due to surface heat fluxes. On the basis of surface fluxes shown in Figure 4, the deepening of the mixed layer with increasing SST comes primarily from the decrease in solar radiative flux and increase in the net surface heat fluxes, $H_e + I_0 + H_s$. The net heat flux into the ocean changes from 50 W m^{-2} to 0 W m^{-2} as SST changes from 24° to 28°C. Corresponding to the reduced heating in the OML, less upwelling is needed to balance the heat budget (equation (8)). For an SST warmer than 28°C, the net heat flux becomes upward and actually cools the OML. Therefore no upwelling can be maintained.

4.2. *Equilibrium States as a Function of Surface Wind*

In this subsection we keep SST fixed at 27°C, representative of the mean tropical Pacific SST, and seek the equilibrium solution for various surface wind speeds. Figure 5*a* shows that the cloud base falls and the cloud top rises with increasing wind. The CBL depth becomes shallower as surface wind weakens, until about 3 m s^{-1}, when an equi-

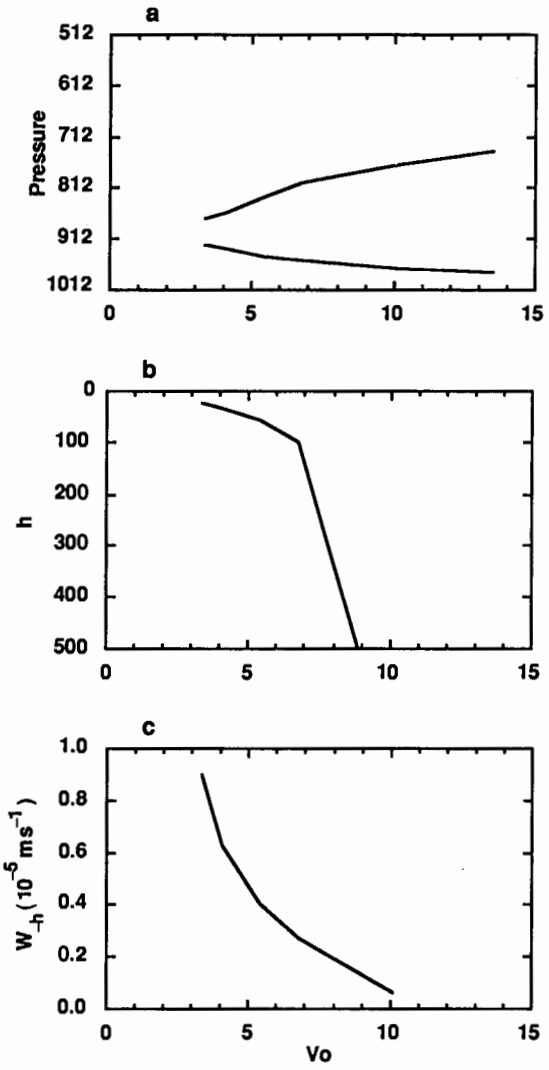

Fig. 5. Same as in Figure 3, but for prescribed SST at 27°C as a function of surface wind.

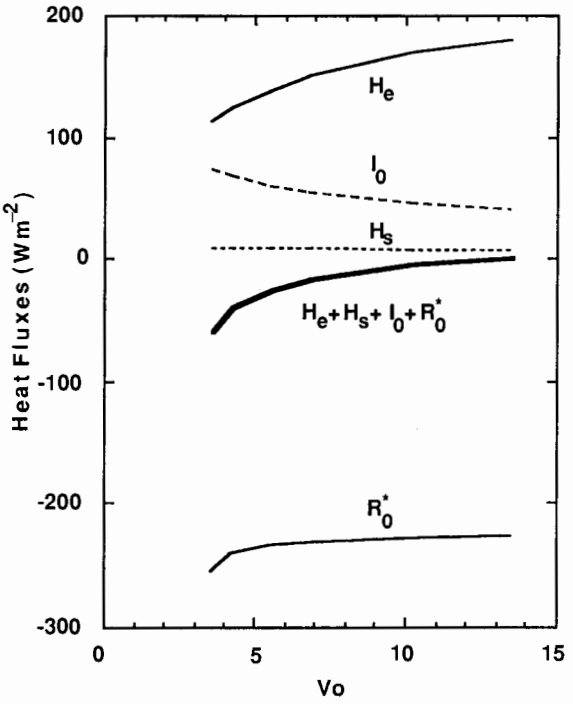

Fig. 6. Same as in Figure 4, but for the prescribed SST at 27°C as a function of surface wind.

librium CBL can no longer be maintained because the subcloud layer becomes too dry due to subsidence above. As the wind increases, the subcloud moisture (q) increases due to increased evaporation. Consequently, θ_e increases with wind speed and approaches θ_{es} of the ocean asymptotically at higher wind speeds (see Figure 5 of BR2).

Figures 5*b* and 5*c* show that the OML deepens, and oceanic upwelling (w_{-h}) decreases with increasing wind. This is caused by the change of surface heat fluxes with wind, as shown in Figure 6. The primary change is the increase of the latent heat flux with increasing wind, which occurs despite a fall of Δq (see section 6). Also significant is the decrease of net longwave radiative flux (I_0) and net solar radiative flux (R_0^*) with increasing wind, due to increased CBL depth and subcloud moisture. As a result, the net heat flux into the ocean becomes less as the wind becomes stronger. Consequently, less upwelling is needed to maintain the heat balance, and a deeper mixed layer results.

4.3. *Equilibrium Solution Corresponding to Observed SST and Surface Wind*

In this subsection we solve the model, with both SST and surface wind prescribed at values representative of the observed January mean SST and 1000-mbar zonal wind of 1979 across the Pacific (Figure 7). In designing the experiment and comparing the model results with observations, we need to keep the major simplifications of our model in mind. For example, horizontal advection is neglected in the coupled boundary layers and both subsidence and fractional cloud cover in the atmosphere is assumed constant across the Pacific, because of a lack of reliable observations. Therefore instead of following observed values in details, a

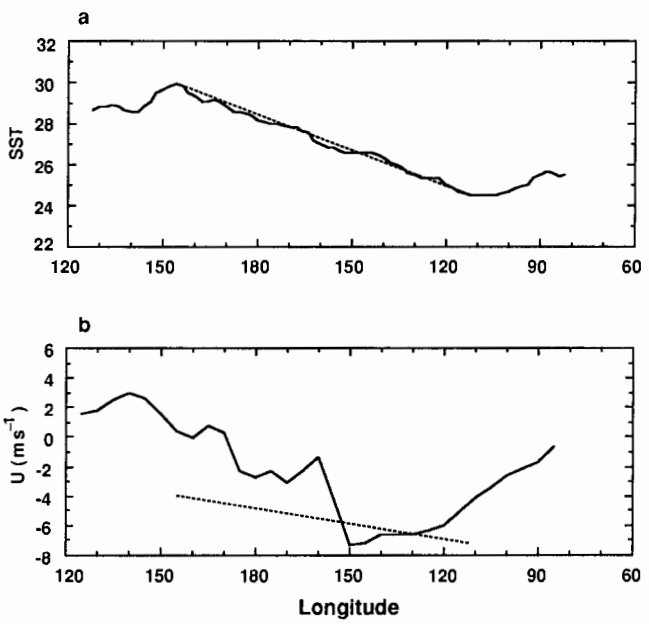

Fig. 7. Zonal distribution of (*a*) January mean SST and (*b*) January mean zonal wind at 1000 mbar, for 1979, along the equator.

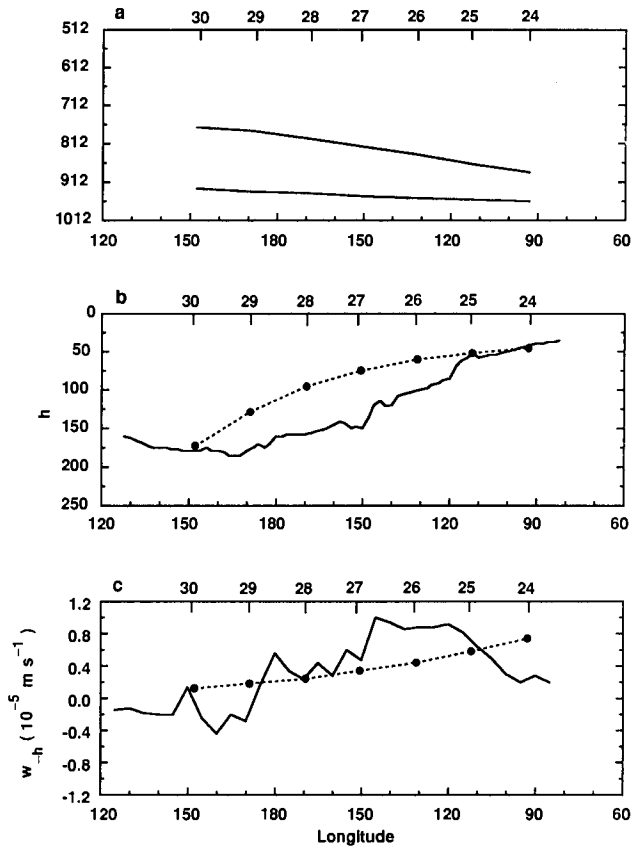

Fig. 8. Equilibrium solution as a function of longitude (or SST) for (*a*) cloud base and CBL top, (*b*) mixed-layer depth (dashed curve), and (*c*) upwelling below the OML (dashed curve), for prescribed SST and surface wind, as shown by dashed lines in Figure 7. The observed D20 and computed $\nabla\cdot(h\mathbf{v}_o)$ (see text) are also shown in Figures 8*b* and 8*c*, respectively.

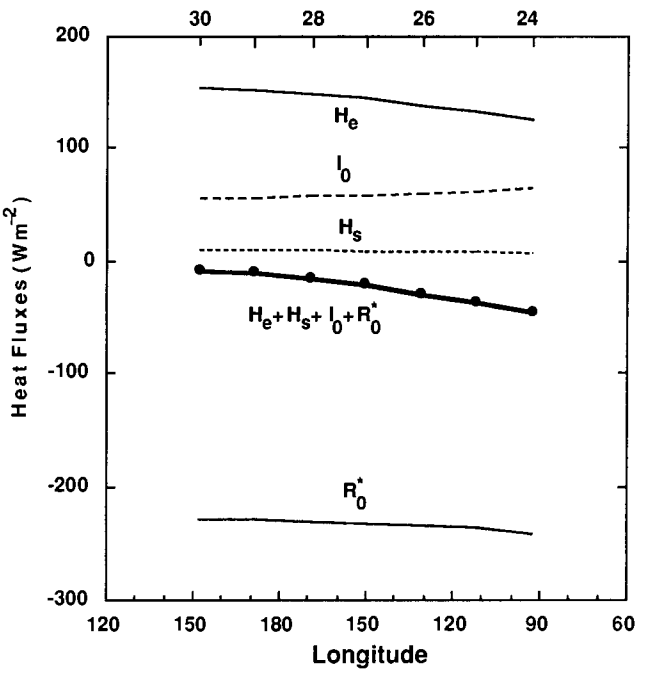

Fig. 9. Surface fluxes for equilibrium solution as a function of longitude (or SST), for prescribed SST and surface wind, as shown by dashed lines in Figure 7.

linear set of SST and surface wind is prescribed, as shown by dashed lines in Figures 7*a* and 7*b*.

The obtained CBL structure, mixed-layer depth, and upwelling as a function of longitude (or SST) are shown in Figure 8. The CBL (Figure 8*a*) is deeper over warmer SST (or toward the western Pacific) due to a more rapid rise of the cloud top than the cloud base as SST increases, in agreement with *Betts and Albrecht* [1987]. The OML depth shown in Figure 8*b* (dashed curve) increases from 50 to 170 m as SST changes from 24°C to about 30°C. Also shown in Figure 8*b* is the climatological (winter) value of the depth of 20°C isotherm (D20) along the equator. The trend of computed h agrees with that of observed h, although a noticeable difference exists in the curvatures of the observed h and computed h in Figure 8*b*. This difference may reflect the effect of zonal variations of subsidence and CBL clouds being neglected in the present experiment. Compared with Figure 3*b*, the mixed-layer depth obtained in the present experiment (Figure 8*b*) is much closer to the observed values west of 150°W over the range of SST between 27° to 30°C, because of weaker surface wind used in this experiment.

The equilibrium solution of w_{-h} is shown in Figure 8*c* (dashed curve). It is noted that the computed w_{-h} is weak where OML is deep (SST is warm), and vice versa. Although oceanic upwelling is obtained from a thermodynamic constraint in our model, it is a dynamic quantity that can also be evaluated directly from the wind field. As a consistency check on the above results, one can integrate the steady horizontal momentum equation

$$f\mathbf{k}\times(\mathbf{v}-\mathbf{v}_g)=\frac{1}{\rho}\frac{\partial\boldsymbol{\tau}}{\partial z}-\gamma\mathbf{v} \tag{12}$$

through the mixed layer from 0 to $-h$ to obtain

$$h\mathbf{v}_o=\frac{1}{\rho_o(f^2+\gamma^2)}(\gamma\boldsymbol{\tau}_0-f\mathbf{k}\times\boldsymbol{\tau}_0+\rho_o f^2 h\mathbf{v}_g+\rho_o f\gamma h\mathbf{k}\times\mathbf{v}_{go}) \tag{13}$$

where

$$\mathbf{v}_g=\frac{1}{f\rho}\mathbf{k}\times\nabla p \tag{14}$$

ρ_o, $\mathbf{v}_o$, and $\mathbf{v}_{go}$ are vertical mean quantities, $\boldsymbol{\tau}_0$ is the surface wind stress, and γ is a dissipation constant.

The frictionally induced vertical velocity at the bottom of the mixed layer, $w(-h)$, is proportional to $\nabla\cdot(h\mathbf{v}_o)$ which can be derived from (13). Using the 1979 January mean wind at 1000 mbar, we compute the contribution to $\nabla\cdot(h\mathbf{v}_o)$ by the surface wind stress, that is, drag and wind stress curl in (13) with γ corresponding to a damping rate of (2 days)$^{-1}$. The estimated $w(-h)$ along the equator is shown in Figure 8*c*. We note that easterly wind (Figure 7*a*) and upwelling prevails over the Pacific east of 170°E and SST ranges from 29° to 24°C in this region. Also noted is the general tendency for upwelling to decrease westward with warmer SST. The equilibrium solution of our model shown in Figure 8*c* is in good agreement with these observations.

The estimated heat fluxes as a function of longitude (or SST) are shown in Figure 9. The magnitude and trend of heat

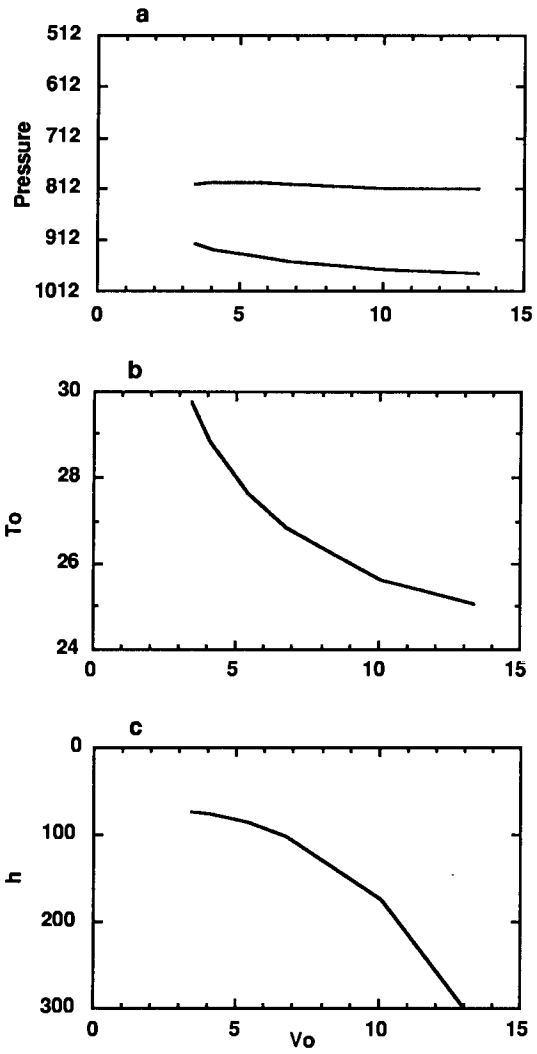

Fig. 10. Same as in Figure 3, but for interactive SST at w_{-h} = 0.27×10^{-5} m s^{-1} as a function of surface wind.

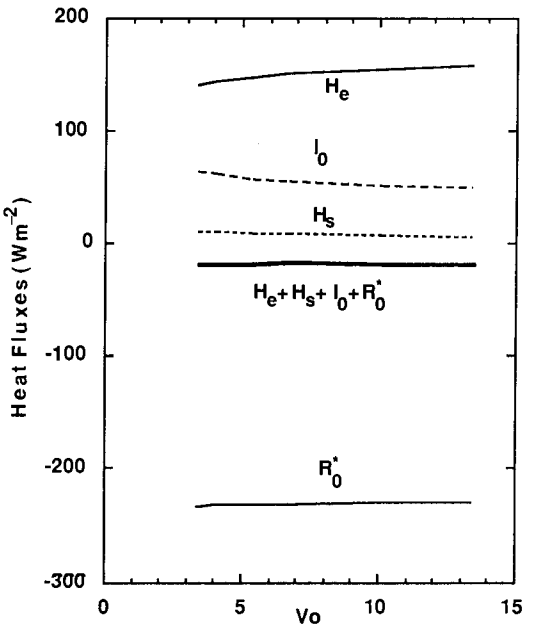

Fig. 11. Same as in Figure 4, but for interactive SST at w_{-h} = 0.27×10^{-5} m s^{-1} as a function of surface wind.

fluxes with SST generally agree with those of observed climatology in the equatorial Pacific [e.g., *Weare et al.*, 1981; *Reed*, 1985].

5. Solutions for Interactive SST in the Coupled Model

In this section we investigate the response of the coupled model to different wind forcings by specifying either w_{-h} or h. Since SST is no longer a prescribed quantity, the equilibrium states are coupled solutions obtained by solving the coupled CBL-OML model iteratively. We choose a set of reference values for T_o, w_{-h}, and h (at 27°C, 0.27×10^{-5} m s^{-1}, and 102 m, respectively) to represent the mean mixed-layer characteristics of the tropical Pacific.

5.1. *Fixed* w_{-h}

The coupled model results shown in Figure 10*a* indicate that the CBL deepens slightly with its top remaining almost constant and base falling with increasing wind. This is the response to the constant w_{-h} constraint. By specifying w_{-h}, we are implicitly requiring a constant net surface heat flux of 16 W m^{-2} into the ocean for different surface wind speeds, according to the thermodynamic equilibrium (7). Under this constraint, SST decreases (Figure 10*b*) and the mixed layer deepens (Figure 10*c*) with increasing surface wind. All these changes with surface winds are accompanied by the changes in surface energy fluxes shown in Figure 11. Since SST tends to cool corresponding to increasing wind speeds, the latent heat flux increases more slowly with surface wind compared with the solution obtained in section 4.2 for fixed SST (Figure 6). The decreasing SST also accounts for the decreasing longwave radiative flux, which offsets the increase of latent heat flux with increasing wind and maintains a constant net heat flux. Note that the downward solar radiative flux only changes slightly with wind.

5.2. *Fixed* h

To maintain a constant mixed layer depth with varying wind, the net surface heat flux into the ocean must increase to reduce the deepening tendency caused by wind increases in (10). To balance the enhanced net heat flux, the coupled system responds in a way that both the CBL top and base fall with increasing wind, accompanied by a sharp drop of SST and increasing upwelling, as shown in Figure 12. The rapid cooling of SST dries the subcloud air causing θ_e to fall quickly (not shown). Therefore the CBL top falls rapidly with increasing wind. Also note that SST decreases almost linearly with increasing wind in Figure 12*b*, while in Figure 10*b*, SST falls more rapidly in the weak wind regime (<5 m s^{-1}) and tapers off as wind becomes stronger and h becomes deeper.

The most surprising result in the heat fluxes, shown in Figure 13, is the decrease of latent heat flux with increasing wind, because here the decrease of Δq (due to reduced SST) overcompensates the increase of wind (see section 6). A significant increase of longwave and solar radiative fluxes in Figure 13 are due to the very dry subcloud and thin CBL depth in high-wind conditions.

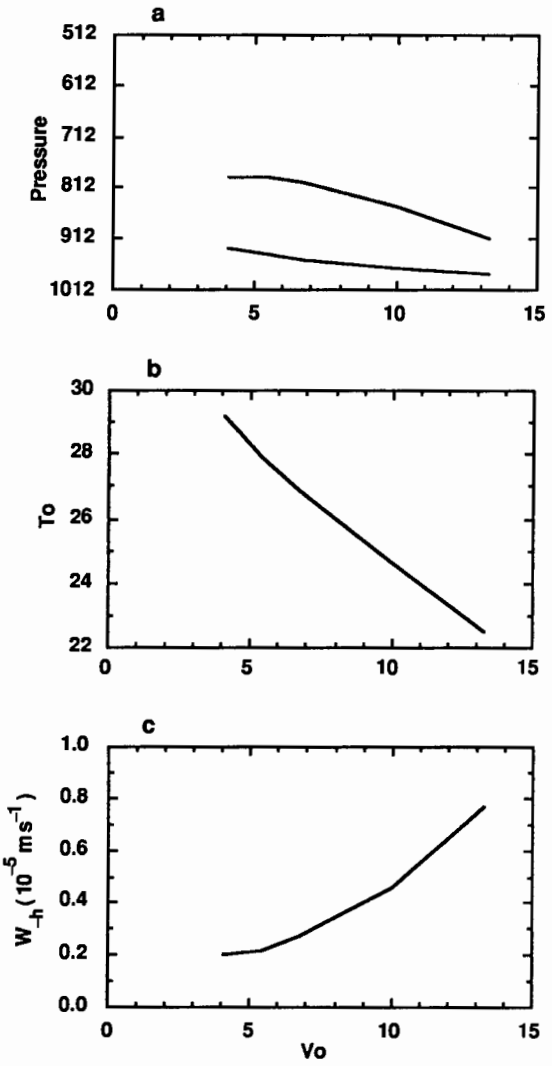

Fig. 12. Same as in Figure 3, but for interactive SST at h = 102 m as a function of surface wind.

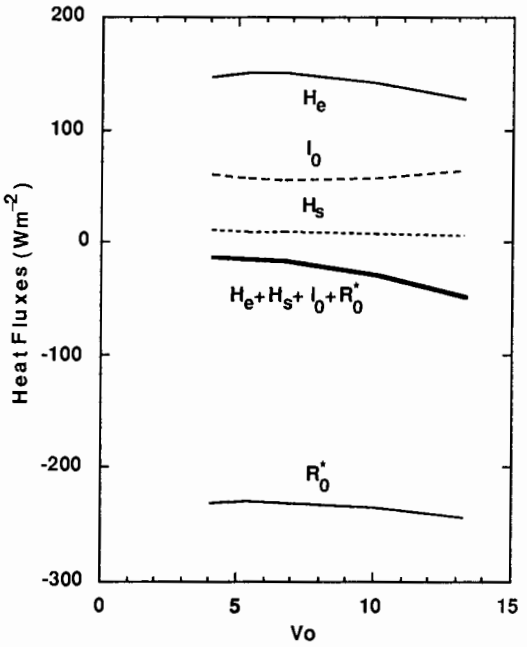

Fig. 13. Same as in Figure 4, but for interactive SST at h = 102 m as a function of surface wind.

5.3. *Observed Surface Wind and w_{-h}*

In subsections 5.1 and 5.2, we discussed the equilibrium solutions of the coupled system as a function of surface wind under two hypothetical conditions in order to systematically understand the response of the coupled system. In nature, both w_{-h} and h would react to the change of surface wind. To illustrate a more realistic response of the coupled system, one can solve the model with prescribed values of surface wind and w_{-h} as a function of longitude, similar to the observed curves across the equatorial Pacific. For example, if the surface wind and w_{-h} are prescribed, as shown in Figures 7*b* and 8*c* (dashed curve), then the model will give the same values of SST and mixed-layer depth, as shown in Figures 7*a* and 8*b* (dashed curve).

6. SUMMARY

From these results, it is obvious that surface energy fluxes are important quantities in the coupled ocean-atmosphere dynamics. Among them, the latent heat flux plays a crucial role in changing the moisture and radiative fluxes in the CBL and the thermodynamic budget in the OML. In sections 4 and 5 we have discussed the effect of latent heat flux on the coupled CBL-OML separately for different conditions. In the following, we concentrate on comparisons of latent heat fluxes under different large-scale controls characterized by SST, surface wind, w_{-h}, and h in the coupled ocean-atmosphere system.

We shall refer to the two prescribed SST experiments discussed in sections 4.1 and 4.2 as case 1 for the fixed surface wind condition and case 2 for the fixed SST condition, respectively. The two interactive SST experiments discussed in sections 5.1 and 5.2 are referred to as case 3 for the fixed w_{-h} condition and case 4 for the fixed h condition, respectively.

Figures 14*a* and 14*b* show the change of Δq and latent heat flux with surface wind for cases 2, 3, and 4. Figure 14*a* shows that the difference of moisture Δq diminishes at higher wind speeds in all three cases, such that the latent heat fluxes in cases 2 and 3 (shown in Figure 14*b*) increase nonlinearly with increasing wind speed. In cases 4, however, the latent heat flux actually decreases with increasing wind, because of the rapid decreasing rate of Δq with respect to wind. On the basis of these hypothetical conditions, our study illustrates that the change of latent heat flux with wind is very sensitive to coupling processes like the evolution of SST, w_{-h}, and h governed by oceanic dynamics.

In Figures 15*a* and 15*b*, we show the change of Δq and latent heat fluxes with SST, corresponding to case 1, the fixed surface wind experiment discussed in section 4.1, and cases 3 and 4, the two wind-varying experiments discussed in sections 5.1 and 5.2. Figure 15*a* shows that Δq is an increasing function of SST in all cases, but its rates of change with SST are very different between the constant wind and varying wind conditions; that is, the rate of change of Δq with SST is larger if the SST change is caused by wind forcing, as in cases 3 and 4. Consequently, depending on the cause of the SST change, the latent heat flux is not neces-

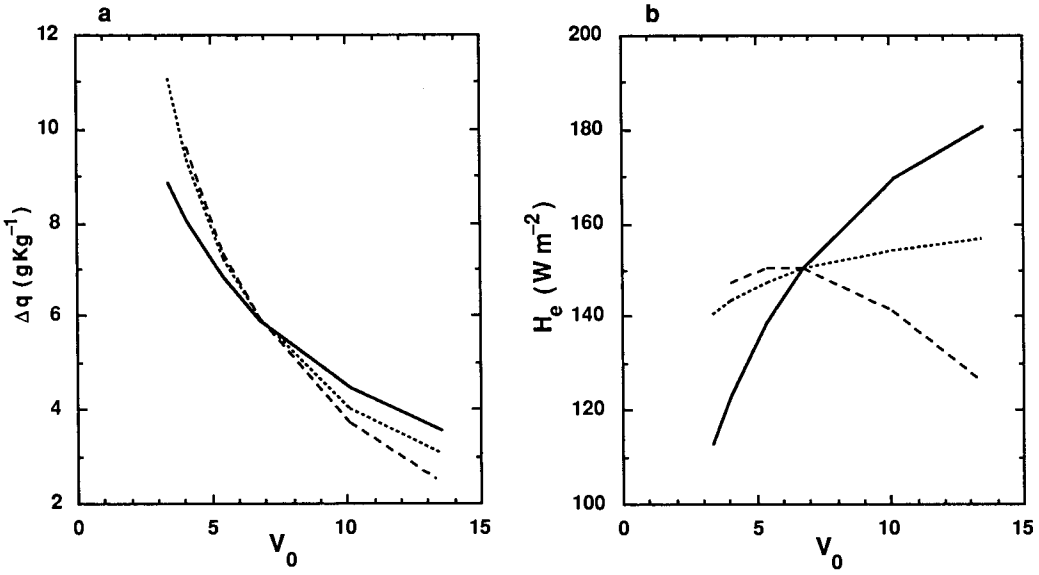

Fig. 14. (*a*) Δq and (*b*) latent heat flux as a function of surface wind for the three solutions: prescribed SST (solid curve), interactive SST at given w_{-h} (dotted curve), and interactive SST at given h (dashed curve).

sarily higher over warmer SSTs: Figure 15*b* shows that the latent heat flux in case 3 decreases with increasing SST (also in case 4 for SSTs warmer than 27°C) because of the very low wind speed. This demonstrates that the change of latent heat flux with SST is dependent on whether the oceanic processes (through w_{-h}, h), or the wind forcing, dominates the SST change.

7. Discussion

In the present study we focus on CBL-OML energy balances, because they are crucial processes in the coupled tropical ocean-atmosphere. The results indicate that the energy balance is extremely sensitive to the change of moisture in the CBL and subcloud layer caused by changes of SST and surface wind. Further studies are needed to advance our understanding of the coupled system. Some of the future work based on the present study is discussed in the following.

The present atmospheric CBL model does not include the effect of precipitation. In fact, annual precipitation over the central and eastern Pacific area is no less than 500 mm [*Taylor*, 1973], which is equivalent to 40 W m^{-2} latent heat released to the deep atmosphere. Apparently, this is a nonnegligible source in the tropospheric energy balance. Through cloud-radiation interaction, the precipitating cloud will profoundly modify the energy balance in the CBL (equation (1)). Precipitation is also an important term in the salinity budget. Inclusion of precipitation and salinity in the coupled model is obviously an immediate step needed to improve our model. In this paper the effect of interactive cloud fraction in the atmospheric CBL model was not consid-

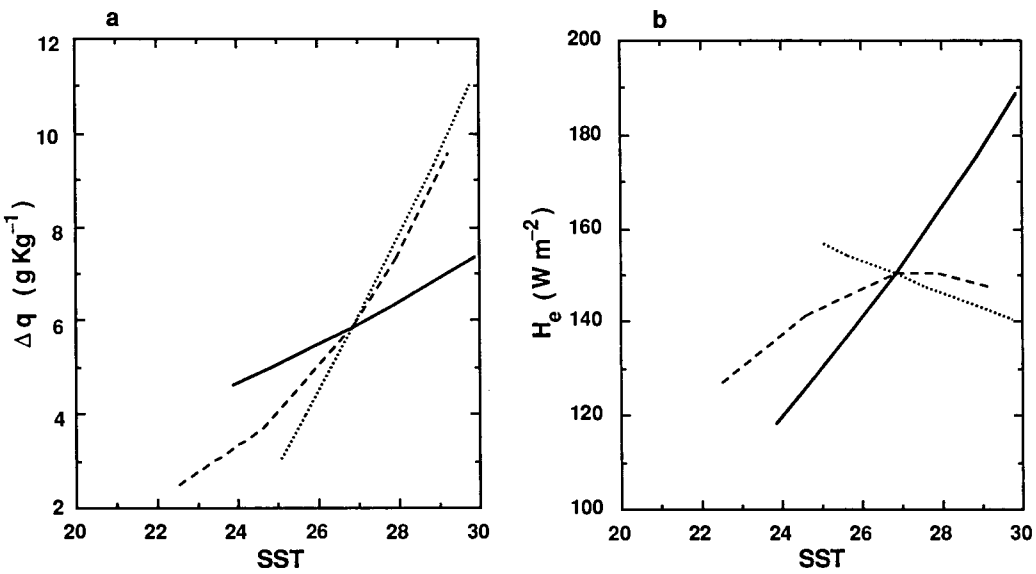

Fig. 15. (*a*) Δq and (*b*) latent heat flux as a function of SST for the three solutions: prescribed SST (solid curve), interactive SST at given w_{-h} (dotted curve), and interactive SST at given h (dashed curve).

ered. Preliminary results indicate that equilibrium solution of the coupled system is quite sensitive to the change of cloud fraction in the CBL model. Since there are many uncertainties about the interactive cloud-radiation processes in the CBL model, improvement in this area may be more difficult.

Because of the limitation imposed by one-dimensional energy balance, meridional and zonal transports are assumed to be small and are ignored in both CBL and OML. Effect of these transports can be included in a more general model framework. Another important assumption in the OML is the closure constraint (10). For a better understanding of the oceanic mixed layer, the parameterization of wind mixing and dissipation need further verification and improvement.

The present model is appropriate for studying the coupled ocean-atmosphere boundary with subsidence above the CBL and upwelling below the OML. To study the interaction in the western Pacific, deep convective processes must be included in the atmospheric model. Large-scale ascending motion in the atmosphere and oceanic downwelling also need to be included in the coupled system. All these are being considered in our ongoing research effort to develop a coupled OML-cumulus ensemble model to study the equilibrium of the coupled ocean-atmosphere in the western Pacific, as well as perturbed climatic states in the coupled system.

8. Conclusion

Motivated by TOGA-COARE, we use a coupled boundary layer model to study the equilibrium state of the ocean-atmosphere in the tropical Pacific region. Our final goal is to understand the coupled processes in the western Pacific warm-pool system. In this paper the equilibrium states of the coupled boundary layer in the central and eastern Pacific are studied as the first step of our research effort. The atmospheric CBL model (developed by *Betts and Ridgway* [1988, 1989]) is composed of a radiation model [*Harshvardhan et al.*, 1987] to calculate radiative fluxes, and three thermodynamic energy balance equations for the subcloud layer and CBL for five variables: H_s, H_e, θ_{M0}, q_{M0}, and θ_T (potential temperature at the top of CBL). The surface fluxes H_s and H_e are parameterized by the bulk formulas in terms of subcloud potential temperature (θ_{M0}), moisture (q_{M0}), surface wind, and SST, where surface wind is prescribed and SST is the major variable of the oceanic mixed layer model. The OML model is composed of the one-dimensional thermodynamic budget equation and a turbulent kinetic energy equation with major variables: SST, w_{-h} (upwelling), and h (mixed layer depth).

Using the coupled model, we study the equilibrium states under different large-scale controls by fixing one of the three variables: SST, w_{-h}, and h. For the prescribed surface conditions discussed in section 4, two sets of experiments are performed to solve for the equilibrium solutions as a function of (1) SST for a given surface wind and (2) surface wind for a given SST. In the interactive SST conditions discussed in section 5, another two sets of experiments are performed to solve for the equilibrium solutions as a function of surface wind for (3) a given w_{-h} and (4) a given h. The following conclusions are reached:

1. For a given set of SSTs at a fixed surface wind, the subcloud air is more moist and the CBL becomes deeper over warmer SST, due to enhanced evaporation from the ocean surface. The moistened and deepened CBL reduces the net surface longwave and solar radiative fluxes. The net surface heat flux decreases with increasing SST, because the increase of latent heat flux (almost linear with increasing SST) is faster than the increase of net (downward) surface radiative flux. The decreased net surface heat flux is balanced by weakened upwelling and is also responsible for increased downward buoyancy in the OML, which causes a deepened OML.

2. Corresponding to a given set of surface winds at a fixed SST, the subcloud is too dry at low surface winds to support an equilibrium CBL. At high surface winds, q_{M0} approaches asymptotically the saturated value, q_o, at sea surface temperature and pressure. Owing to the nonlinear change of $(q_o - q_{M0})$ with increasing surface wind, the rate of increase of latent heat flux is slower at high wind speeds than at low wind speeds. The resultant high θ_e in the subcloud layer favors a deep CBL, which reduces the downward solar radiation and increases the downward longwave radiation at the surface. The net surface heat flux decreases with increasing wind, and leads to a weaker upwelling and deeper OML.

3. For a given set of surface winds at a fixed w_{-h}, the total surface heat flux is constrained to remain constant to balance the upwelling (7). Corresponding to increasing wind speeds, SST is found to decrease, and the CBL base falls slightly. But the CBL top remains almost constant, so that the solar radiative flux also remains unchanged. Thus the major heat balance is essentially maintained between the latent heat flux and longwave radiative flux. Since the generation of turbulent kinetic energy by thermal buoyancy remains constant, the OML depth simply deepens with a stronger surface wind.

4. For a given set of surface winds at a fixed h, the total heat flux into the ocean must increase (downward buoyancy decrease) to balance the increased turbulent kinetic energy due to increasing wind. SST again decreases with increasing wind, as in case 3. However, the fall of SST is much faster in case 4, because the mass of water is fixed, whereas in case 3 the mixed layer is allowed to deepen, and the cooling is spread over a larger mass of water. The rapid decrease in SST causes a decreasing latent heat flux (evaporation) and CBL depth with increasing wind, because of the rapid decrease of moisture in the CBL.

To further compare the validity of our model, we carried out additional experiments based on observed conditions. In the prescribed SST experiment, we specified a set of SST and surface wind similar to the observed values across the Pacific. In the interactive SST experiment, we prescribed a set of surface wind and w_{-h} based on observations along the equator. The magnitude and zonal gradient of the equilibrium solutions from these experiments are in general agreement with the observed climatology across the Pacific. This illustrates the usefulness of our simple model as a tool to study the surface energy balance in the coupled tropical ocean-atmosphere.

Appendix

The Upper Boundary Fluxes in OML

$$|\overline{(w'\mathbf{v}')_0}| = \frac{|\boldsymbol{\tau}_0|}{\rho_o} \equiv u_*^2 \tag{A1}$$

$$\overline{(w'T')_0} = \frac{1}{\rho_o c}(I_0 + H_s + H_e) \tag{A2}$$

$$\overline{(w'S')}_0 = \frac{1}{\rho_o}(P - E)S_o \tag{A3}$$

By defining buoyancy (B) as

$$B = -g\frac{\rho'}{\rho} = g\alpha T' - g\lambda S' \qquad \alpha = -\frac{1}{\rho}\frac{\partial \rho}{\partial T},\ \lambda = \frac{1}{\rho}\frac{\partial \rho}{\partial S} \tag{A4}$$

The buoyancy flux can be derived as

$$\begin{aligned} F_{B0} &= \overline{(w'B')}_0 \\ &= g\alpha\overline{(w'T')}_0 - g\lambda\overline{(w'S')}_0 \\ &= \frac{g\alpha}{\rho_o c}(I_0 + H_s + H_e) - \frac{g\lambda}{\rho_o}(P - E)S_o \end{aligned} \tag{A5}$$

The Lower Boundary Fluxes in OML

The thermodynamic and salinity equations can be expressed as

$$\frac{\partial \varphi}{\partial t} + w\frac{\partial \varphi}{\partial z} + \frac{\partial}{\partial z}\overline{w'\varphi'} = \sigma_\varphi \tag{A6}$$

The buoyancy equation can also be expressed in the same form by combining the thermodynamic and salinity equations. Here φ denotes T, S, or B and

$$\sigma_s = 0 \qquad \sigma_T = -\frac{1}{\rho c}\frac{\partial R^*}{\partial z} \qquad \sigma_B = -\frac{g\alpha}{\rho c}\frac{\partial R^*}{\partial z} \tag{A7}$$

The equation can be vertically integrated from $-h - \delta h$ to $-h$ to yield

$$\begin{aligned} &\frac{\partial}{\partial t}\int_{-h-\delta h}^{-h} \varphi\, dz - \varphi_{-h-\delta h}\frac{\partial}{\partial t}\delta h \\ &\quad + \left(w_{-h} + \frac{\partial h}{\partial t}\right)(\varphi_o - \varphi_{-h-\delta h}) + \overline{(w'\varphi')}_{-h} \\ &\quad - \overline{(w'\varphi')}_{-h-\delta h} = \int_{-h-\delta h}^{-h} \sigma_\varphi\, dz \end{aligned} \tag{A8}$$

If $\overline{w'\varphi'}$ is negligible at $z = -h - \delta h$ (immediately below the mixed layer) and φ is assumed to be steady within the entrainment zone, then in the limit as δh approaches zero, (A8) gives the entrainment expression as

$$\overline{(w'\varphi')}_{-h} = -\Lambda\left(w_{-h} + \frac{dh}{dt}\right)(\varphi_o - \varphi_{-h}) \tag{A9}$$

where Λ is the Heaviside step function having the properties that $\Lambda = 0$ if $(w_{-h} + dh/dt) < 0$, otherwise $\Lambda = 1$. The entrainment flow can only be directed toward the more turbulent fluid region. Therefore it is associated with layer deepening in the present considerations. When the layer becomes shallower, the entrainment must cease. The symbol Λ is introduced as a switch to turn on or off the entrainment effect.

Turbulent Kinetic Energy

The horizontally homogeneous turbulent kinetic energy equation can be approximated as

$$\frac{\partial k}{\partial t} = -\overline{w'\mathbf{v}'}\frac{\partial \bar{\mathbf{v}}}{\partial z} - \frac{\partial}{\partial z}\left(\overline{w'k} + \frac{1}{\rho}\overline{w'p'}\right) + \overline{w'B'} - \varepsilon \tag{A10}$$

where $k = \frac{1}{2}(u'^2 + v'^2 + w'^2)$.

The first term on the right-hand side of (A10) represents generation of turbulent energy due to the work of the Reynolds stresses on the mean shear flow. It expresses conversion from the mean kinetic energy. The turbulent energy is likely to be generated by the mixing of shear flows primarily near the top and bottom of the mixed layer, even in conditions of horizontal homogeneity. The second term is the convergence of the turbulent vertical energy flux. At the surface, this flux can be associated with the wind stress multiplied by a wind velocity from dimensional considerations. Near the bottom of the mixed layer, this flux may be expressed in some form of entrained turbulent kinetic energy. The derivation of an explicit expression for the flux and generation of turbulent kinetic energy requires additional momentum information. Here we shall just assume that the vertical integration of these two terms is proportional to u_*^3.

The third term in (A10) represents the rate of work done by the buoyancy force, and represents conversion from the mean potential energy. The vertical integration of the buoyancy flux can be derived from the buoyancy equation (A6) as

$$\begin{aligned} \int_{-h}^{0} \overline{w'B'}\, dz = \tfrac{1}{2}hF_{B0} - \tfrac{1}{2}\Lambda\left(w_{-h} + \frac{dh}{dt}\right)B_{\delta h}h + \frac{g\alpha}{\rho_o c} \\ \cdot\left[\frac{h}{2}R_0^* + \frac{h}{2}R_{-h}^* - \int_{-h}^{0} R^*\, dz\right] \end{aligned} \tag{A11}$$

where

$$B_{\delta h} = g\alpha(T_o - T_{-h}) - g\lambda(S_o - S_{-h}) \tag{A12}$$

The last term of (A10) is the rate of dissipation of turbulent energy. This is the most uncertain term. A possible treatment is proposed by *Niiler and Kraus* [1977], who assume that the dissipation integral is composed of terms which are individually proportional to the active turbulence generating processes. For the present, we simply assume that the dissipation only exists in the generating processes related to the working of the wind. Therefore the following relation is derived:

$$\int_{-h}^{0}\left\{\frac{\partial}{\partial z}\left(\overline{w'k} + \frac{1}{\rho}\overline{w'p'}\right) + \overline{w'\mathbf{v}'}\frac{\partial \bar{\mathbf{v}}}{\partial z} + \varepsilon\right\} = -mu_*^3 \tag{A13}$$

Acknowledgments. The authors would like to thank W. Ridgway for providing the atmospheric CBL model for use in this work. Discussion with L. Peng is gratefully acknowledged. C.-H. Sui is supported through a NASA-NRC Resident Research Associateship at the Goddard Space Flight Center. A. K. Betts is supported by NASA Goddard Space Flight Center under contract NAS5-30524 and the National Science Foundation under grant ATM90-01960.

REFERENCES

Betts, A. K., Saturation point analysis of moist convective overturning, *J. Atmos. Sci.*, *39*, 1484–1505, 1982.

Betts, A. K., Mixing line analysis of clouds and cloudy boundary layers, *J. Atmos. Sci.*, *42*, 2751–2763, 1985.

Betts, A. K., and B. A. Albrecht, Conserved variable analysis of the convective boundary thermodynamic structure over the tropical oceans, *J. Atmos. Sci.*, *44*, 83–99, 1987.

Betts, A. K., and W. Ridgway, Coupling of the radiative, convective and surface fluxes over the equatorial Pacific, *J. Atmos. Sci.*, *45*, 522–536, 1988.

Betts, A. K., and W. Ridgway, Climatic equilibrium of the atmospheric convective boundary layer over a tropical ocean, *J. Atmos. Sci.*, *46*, 2621–2641, 1989.

Chu, P. C., and R. W. Garwood, Jr., Cloud-ocean mixed layer feedback, in *Symposium on the Role of Clouds in Atmospheric Chemistry and Global Climate*, preprint vol., pp. 39–44, American Meteorological Society, Boston, Mass., 1989.

Denman, K. L., A time-dependent model of the upper ocean, *J. Phys. Oceanogr.*, *3*, 173–184, 1973.

Harshvardhan, R. Davies, D. A. Randall, and T. G. Corsetti, A fast radiation parameterization for atmospheric circulation models, *J. Geophys. Res.*, *92*, 1009–1016, 1987.

Kim, J.-W., A generalized bulk model of the oceanic mixed layer, *J. Phys. Oceanogr.*, *6*, 686–695, 1976.

Kraus, E. B., and J. S. Turner, A one-dimensional model of the seasonal thermocline, II, The general theory and its consequences, *Tellus*, *19*, 98–106, 1967.

Latif, M., J. Biercamp, and H. von Storch, The response of a coupled ocean-atmosphere general circulation model to wind bursts, *J. Atmos. Sci.*, *45*, 964–979, 1988.

Meyers, G., Annual variation in the slope of the 14°C isotherm along the equator in the Pacific ocean, *J. Phys. Oceanogr.*, *9*, 885–891, 1979.

Miller, J. R., The salinity effect in a mixed layer ocean model, *J. Phys. Oceanogr.*, *6*, 29–35, 1976.

Niiler, P. P., and E. B. Kraus, One-dimensional models of the upper ocean, in *Modeling and Prediction of the Upper Layers of the Ocean*, edited by E. B. Kraus, pp. 143–172, Pergamon, New York, 1977.

Reed, R. K., An estimate of the climatological heat fluxes over the tropical Pacific ocean, *J. Clim. Appl. Meteorol.*, *24*, 833–840, 1985.

Sarachik, E. S., Tropical sea surface temperature: An interactive one-dimensional atmosphere-ocean model, *Dyn. Atmos. Oceans*, *2*, 455–469, 1978.

Taylor, R., An atlas of Pacific rainfall, *Rep. HIG-73-9*, Hawaii Inst. of Geophys., Honolulu, 1973.

U.S. TOGA-COARE Science Working Group, TOGA-COARE science plan, Univ. Corp. for Atmos. Res., Boulder, Colo., July 1989.

Weare, B. C., P. T. Strub, and M. D. Samuel, Annual mean surface heat fluxes in the tropical Pacific ocean, *J. Phys. Oceanogr.*, *11*, 705–717, 1981.

A. K. Betts, RD 2, Box 3300, Middlebury, VT 05753.

K.-M. Lau and C.-H. Sui, Laboratory for Atmospheres, Code 913, NASA Goddard Space Flight Center, Greenbelt, MD 20771.

(Received March 5, 1990;
accepted June 26, 1990.)